Nickel Oxide Photocathodes Prepared Using Rapid Discharge Sintering for *p*-Type Dye-Sensitized Solar Cells

[1,2]Muhammad Awais,* [1,3]Danilo Dini, [1]Johannes G. Vos and [1,4]Denis P. Dowling
[1]Solar Energy Conversion Strategic Research Cluster, Dublin, Ireland.
[2]Gulf Organization for Research and Development, QSTP, Doha, Qatar.
[3]Department of Chemistry, University of Rome "La Sapienza", Rome, Italy.
[4]School of Mechanical and Materials Engineering, University College Dublin, Ireland.
m.awais@gord.qa*

Summary: This paper compares the photoelectrochemical performances of nickel oxide (NiO) thin films processed using two different sintering procedures: rapid discharge sintering (RDS) and conventional furnace sintering (CS). Prior to sintering, NiO nanoparticles were sprayed onto substrates to form loosely adherent nanoparticulate coatings. After RDS and furnace sintering the resultant NiO coatings were sensitized with erythrosine B dye and corresponding p-type dye-sensitized solar cells were fabricated and characterized. NiO electrodes fabricated using the RDS technique exhibited a fourfold enhancement in electroactivity compared to CS electrodes. A possible explanation is the smaller sintered grain size and more open mesoporous structure achieved using the microwave plasma treatments.

Keywords: NiO; *p*-type semiconductor; Dye-sensitized solar cells; Rapid discharge sintering; Electroactivity.

Introduction

Man-made climate change is becoming one of the most important threats to humanity. This is highlighted by the fact that only recently CO_2 concentrations in the atmosphere have reached values around 400 ppm. There is therefore a need for the development of novel energy technologies that are carbon neutral rather than based on fossil fuels. The sun constitutes an important renewable energy as the total power from sunlight striking the ground is enormous about 10^5 TW per year. Even if not all this energy can be harvested sufficient energy from sunlight can be generated in order to meet the growing energy demands of the world's population, which is presently of the order of 15 TW per year [1]. Historically the first photovoltaic cell created by a team at Bell Laboratories in 1954 [2] opened a new dimension in the exploitation of solar energy for the production of electricity through the use of *p-n* junctions of crystalline Si. The successive generation of photovoltaic devices consisted of thin film solar cells including amorphous silicon (a-Si), cadmium telluride (CdTe) and copper indium gallium diselenide (CIGS) as photoactive materials [3]. Dye-sensitized solar cells (DSCs) appeared in relatively newer [4] as a low-cost photoelectrochemical alternative to the photovoltaic devices based on *p-n* junctions. The use of nanoporous titanium oxide TiO_2 in the anatase crystalline form with a roughness factor of *ca.* 1000, dramatically increased the light harvesting efficiency of the TiO_2-based electrode and resulting solar cells with an efficiency as high as 7 % were reported by O'Regan and Grätzel [4]. For the last twenty year or more there was a limited increase in the efficiency of DSCs (also known as the Grätzel cells), [5]. Recently with the advent of perovskite-sensitized solar cells the efficiency of these types of cells has gone beyond 20 % [6-11]. However, this top value is somehow limited when compared to the performance of Si-based photovoltaic devices.

A method of exploiting the solar spectrum more effectively was introduced by He *et al* [12] who placed dye-sensitized *p*-type semiconductor, giving photoelectrochemical response, as a substitute of a non photoactive cathode of a conventional DSC [13]. By joining anode and cathode that are both photoactive, the resulting DSC will assume a tandem configuration [12]. The latter device has the capacity to harvest an increased segment of the solar spectrum when compared to a normal DSC provided that the dyes sensitizing the two different electrodes have complementary absorption spectra. It is expected that a tandem DSC's efficiency (hypothetical higher value) is approximately 13 % more when compared with DSC having only one photoactive electrode [12].

For the conversion of the solar radiation into electrical energy with a cathodic DSC (or *p*-DSC) that works through the photoactivation of a reduction process [12,14], the main prerequisite is the preparation of a *p*-type semiconductor with mesoporous morphology that chemisorb high amounts of dye sensitizers and create an extended

---

*To whom all correspondence should be addressed.

electrochemical interface with the electrolyte (*vide infra*) [15]. There is a potential application of *p*-type semiconductor also as a doping agent for the hole transport medium (HTM) in perovskite-sensitized solar cells [6, 7, 16]. Nickel oxide (NiO) was chosen as cathodic semiconducting material because of its *p*-type nature [17], high chemical stability, and well defined optical/electrical properties [18]. NiO possesses broad band-gap energy ranging from 3.4 to 4.0 eV according to the presence of defects in the lattice, chemical composition and crystalline phase [17]. NiO coatings can be deposited with various techniques like plasma enhanced chemical vapor deposition [19, 20], spray pyrolysis [21, 22], pulsed laser deposition [23, 24], electrodeposition [25], chemical bath deposition [21, 26], sol-gel [12, 14, 15, 27-29], sputtering [30, 31], and hydrothermal synthesis [25, 32]. Exempting electrochemical techniques [33], the chemical methods of deposition generally need post thermal treatments for increasing the density and the viscosity of the coatings through the removal of the reaction medium, and to define the crystal phase(s) of the NiO coating [34]. Typical the NiO thermal sintering temperatures are in the range 350-550°C [27, 33, 35, 36] with sintering times of 30-60 min.

The objective of this study is to prepare *p*-type NiO coatings with the help of plasma supported microwave sintering for use in *p*-DSCs as photocathodes. The advantages of microwave plasma sintering include the significant reduction of the cycle times [37], and the decrease of electrical power used during the sintering treatment. In addition, microwave plasma sintering treatments have been applied as it can facilitate more homogenous heating [38] with nanoporous textures, which enjoin increased interconnectivity between nanoparticles keeping a consistent contact at the NiO coating/substrate interface. These characteristics diminish the inherent confrontation of the metal oxide structure and permit proficient alliances of charge carriers at substrate and NiO contact of the photocathode. Moreover, the nanoporous morphology of the *p*-type electrode permits the adsorption of greater amounts of dye per unit area regarding a compact layer, and favors injection of the charge from the sensitizer to the photocathode in the whole film. This should results into the increase of the photocurrent as a result of oxide film thickness [39]. In the present study NiO surfaces prepared by a novel rapid discharge sintering (RDS) method are judged against conventional furnace sintering techniques (CS). The electrode surfaces are investigated by both electrochemical and surface techniques and their ability to act as solar cathodes

using erythrosine B (ERY) as a dye-sensitizer are compared.

Experimental

NiO Coating Deposition

The NiO layer was deposited using spraying technique with fluorine doped tin oxide (FTO) glass substrates (12 Ω/sq, 3 mm thick) procured from Solaronix. Prior to spray of NiO particulate layer, the substrates (2 x 2 cm) were cleaned using ultrasonication in methanol followed by acetone. Each cleaning step of the substrate was 5 min long. The NiO nanoparticles 50 nm in size (99.8 % grade from Sigma-Aldrich) were mixed in 2-propanol in order to prepare a suspension with the mass concentration of 20 mg mL^{-1}. The particulate layer of NiO was deposited via to and fro spraying technique [40]. The microwave assisted plasma sintering technique also called as rapid discharge sintering (RDS) was performed with the help of a circumferential antenna plasma (CAP) microwave system as detailed elsewhere [41]. The plasma was obtained at a pressure of 5 mbar in an Ar and O_2 (10:1) ambiance. For the development of plasma, input powers of 2.4 kW were formed by a Mugge microwave power supply working at a frequency of 2.45 GHz. The temperature of the working specimens were measured in-situ during the heat treatment with a LASCON QP003 two-color pyrometer made by Dr Merganthaler GmbH & Co. The conventional sintering (CS) were performed in air with a Carbolite Furnace (RHF 1200). Three NiO samples were sintered concurrently at ~450 ºC temperature for both furnace and microwave plasma sintering processes, for durations of 60 and 5 min, respectively [39]. The thickness of NiO coatings were controlled with the help of spraying passes [39]. NiO coatings having minimum thickness of 0.6 μm are acquired using one pass while thicker samples were prepared using numerous back and forth passes of nanoparticles (in suspension) spraying. The NiO samples attained with several passes generally exhibited a non homogeneous thickness.

Characterization Studies

The thickness of NiO coatings was estimated using step height measurement technique with the help of an optical profilometer (WYKO NT1100) in the vertical scanning interferometry (VSI) mode. For carrying out the morphological analysis and cross sectional examinations, the samples were inspected with FEI Quanta 3D FEG DaulBeam system (FEI Ltd, Hillsboro, USA). BET isotherms were performed with the help of ASAP 2420 from Micromeritics, Norcross, GA, USA under

krypton (Kr) atmosphere. NiO particles were deposited and sintered onto ca. 0.5 cm x 1 cm FTO glass substrates using methods described above. Three number of samples prepared under same cnditions were inserted into glass sample tubes. In order to remove moisture and other adsorbed gases the samples were degassed under vacuum at 25 °C for 3 hours. Krypton isotherms were obtained at relative pressure (p/p^0) of 0.07-0.2 at –195.85 °C in liquid nitrogen (N$_2$). The glass samples were then weighed and reweighed following the removal of the NiO in order to give an accurate sample weight. BET isotherms were fitted using Microactive (Micrometrics Instrument Corporation). NiO coatings were immersed in a mixture of 0.3 mM erythrosine B (ERY) sensitizer [12,33], in an ethanol (99.8 %) solution overnight. To assemble *p*-type DSCs, the coatings with sensitizer were joined with a platinum coated FTO counter electrode in the face-to-face arrangement, with the help of customized shapes Surlyn® tape. The prepared structure was packed with 0.5M I$_2$, 0.05M LiI in acetonitrile as electrolyte from a pre-drilled hole in the counter electrode under low pressure. The hole was later packed with Surlyn® and a glass slide. For *J-V* characteristics calculations the coatings were veiled using a 4 x 4 mm opaque frame and during all measurements front illumination mode were observed using a solar simulator with AM1.5G spectral distribution. The simulator was calibrated using a certified reference cell with an intensity of 87 mW cm^{-2}. The redox properties of NiO electrodes were investigated using a special cell with a three-electrode arrangement: bare NiO (deposited onto FTO) and dye-sensitized NiO were the working electrodes, whereas two Li rods (Sigma-Aldrich) were utilized as reference and counter electrode, respectively. More details of this cell are reported elsewhere [42].

Results and Discussion

Fig. 1 shows the type of glass slides onto which the loosely adherent NiO particulate layers were deposited. A slurry made of metal oxide nanoparticles in 2-propanol (20 mg mL^{-1}) was used for spraying. The coating thicknesses were maintained in the range 0.6-3.0 μm by controlling the number of spraying runs. The NiO coating thickness was evaluated with an optical profilometer that measured the step height (Fig. 2). In order to enhance the electrical connectivity between the loosely adherent NiO nanoparticles, two different sintering methods were adopted: Rapid discharge sintering (RDS samples) [39, 43], and conventional furnace treatment (CS samples) [43]. Previous studies have demonstrated that for the RDS procedure the optimum sintering time is 5 min [43] because it

affords the percolation of the oxide nanoparticles all the way through the coating structure while preserving mesoporosity. Moreover, it provides a homogeneous electrical connection at the FTO/NiO boundary. It was also proved previously[43] that smaller crystallite size calculated from XRD examinations resulted into increased dye-absorption for the case of RDs treated NiO coatings. The BET isotherms analysis of these thin film electrodes gave a surface area of about 20 and 8 m^2 g^{-1} for RDS and CS samples, respectively. The morphological features obtained allow for a homogeneous sensitization of the entire oxide layer and high overall photocurrent efficiencies (η) [39]. Fig. 3 shows the time profile of the temperature of the NiO coating during the RDS treatment. In the RDS procedure the extent of mesoporosity can be controlled by changing the duration of sintering. NiO coatings which are optimally sintered would facilitate diffusion of the electrolyte right through the entire coating and photactivated charge injection is thus realized for the entire electrode surface. NiO coating samples treated using RDS for periods up to 10-60 min produce lower grade for the photovoltaic performance in comparison to the coatings sintered for 5 min as show below [43]. It is due to prolonged sintering time induces the steady closure of the pores with the grain size enlargement and reduction in surface area that consequently reduces the amount of dye adsorbed on its surface. In order to compare RDS treated coatings with those obtained from conventional furnace treatments, also the NiO coatings of the CS type (*vide supra*) were sintered at 450 °C with the same sintering time of 5 min inside the furnace. The heating and cooling rate were 10 °C min^{-1}. A total cycle time of ~120 min was required for the furnace sintering CS, in contrast using the RDS technique the entire processing time including pump down, thermal treatment and cooling, took only 15 min.
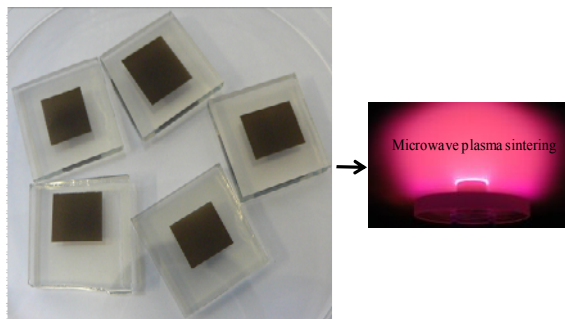

Fig. 1:   NiO layers (thickness of 2 to 3 μm, area: 1 x 1 cm^2), directly after spray deposition onto the FTO-coated glass substrates prior to microwave plasma sintering (shown).
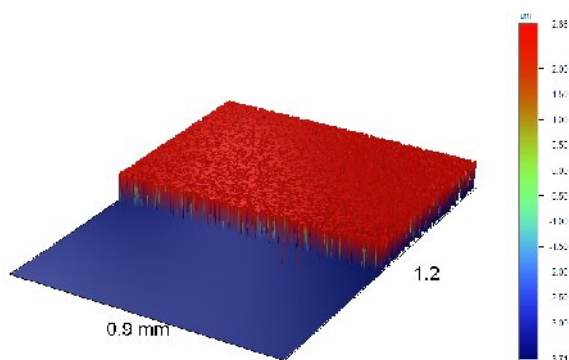
Fig. 2:   Optical profilometer image of a 2.5 µm thick NiO film obtained via step height measurement.
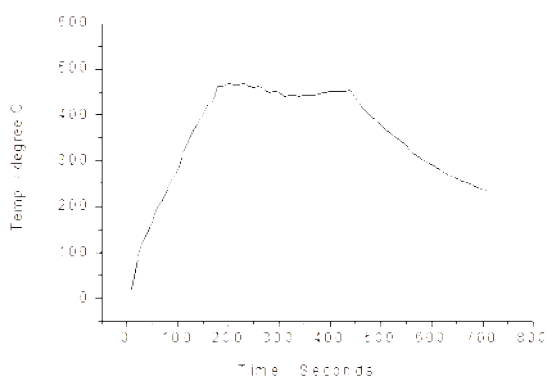

Fig. 3:   Temperature profile obtained using optical profilometry during RDS treatment of the NiO layer.

Electrochemical Properties of RDS and CS Samples

The electrochemical properties of the sintered NiO samples were analyzed with cyclic voltammetry when NiO was in the bare (Fig. 4) and ERY-sensitized (Fig. 5) state. These electrochemical characterizations were conducted in a three-electrode cell [42]. The purpose of these experiments was to investigate the electrochemical properties of the NiO coatings. Moreover, the electrochemical properties of bare and dye-sensitized NiO coatings, sintered using the two treatments, were compared [44]. From the integration of the anodic currents observed in the cyclic voltammograms in Fig. 4, a 7.86 mC cm^{-2} anodic charge was measured for RDS treated bare NiO coatings.[42] In contrast the values for the furnace sintered coatings were only 3.96 mC cm^{-2}. The resulting ratio of the charge exchanged for the RDS treated NiO to that of furnace sintered NiO was therefore approximately 2:1. The NiO oxidation was found to be fully reversible for both NiO coatings sintered using both techniques (Fig. 4). The twofold increase in the electrochemical activity for NiO coatings prepared using the RDS technique,

compared with that for the furnace sintered coatings is likely to be associated with the smaller grain size and more porous structure of the RDS sintered oxide coating compared to those that were furnace sintered. This is demonstrated based on the SEM images shown in Fig.s 6 and 7 for the RDS and CS sintered oxides respectively. Despite having the same starting NiO powders with mean particle size of 50 nm, the average grain size (15 measurements) obtain for the RDS NiO is ~25 nm while that for the CS is ~45 nm. The FEG-SEM images also demonstrate the denser more closed porosity for the latter coatings. This combined with the smaller surface area due to the larger NiO particle agglomerates obtained using furnace sintering would explain their reduction in performance. It has previously been highlighted that the higher level of particle interconnectivity and enhanced adhesion of the NiO film to the substrate achieved using the RDS treatment *vs* the CS procedure also helps the former to yield enhanced conductivity [43]. It is found that the type of sintering affects mainly the current density for the both types of NiO coatings with equal thickness (Fig. 4), however does not change the characteristics of the redox processes based on Ni^{2+} as main electroactive species [39,43]. For both RDS, and CS samples the main reversible oxidation peak of NiO is located at 3.3 V *vs* Li$^+$/Li, and the current wave with shoulder appearance falls in the range 2.5-3.0 V *vs* Li$^+$/Li in the voltammograms of both bare NiO samples (Fig. 4). These common electrochemical features indicate the presence of Ni^{2+} in two different coordination environments in NiO samples, [39] and reveal analogous chemical composition for the two differently sintered NiO films[43].
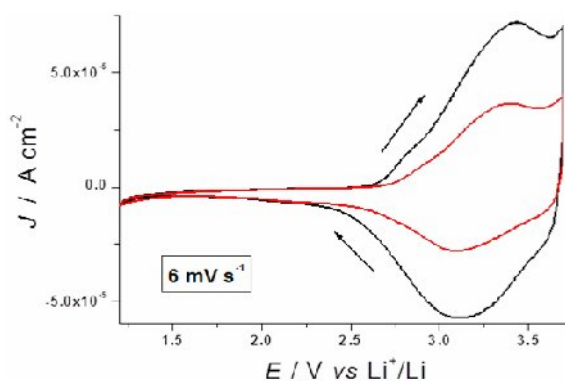

Fig. 4:   Cyclic voltammograms of (black trace) RDS and (red trace) furnace sintered NiO coatings (thickness: 2.5 µm) in the potential range of NiO oxidation. Electrolyte composition: 0.5 M LiClO$_4$ in anhydrous propylene carbonate; scan rate: 6 mV s^{-1}.
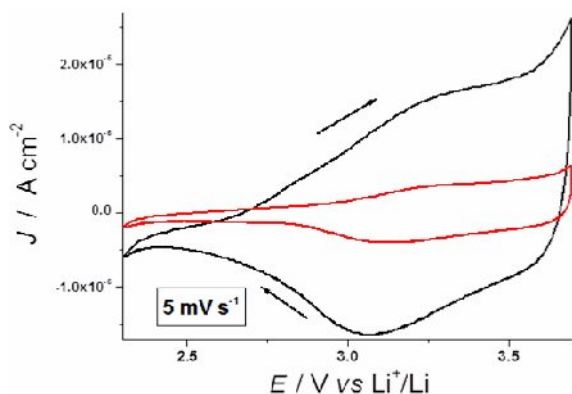
Fig. 5: Dark cyclic voltammograms of (black trace) RDS and (red trace) furnace sintered NiO coatings sensitized with ERY (thickness: 2.5 μm). The selected range of applied potential brings about the oxidation of NiO. Electrolyte composition: 0.5 M $LiClO_4$ in anhydrous propylene carbonate; scan rate: 5 mV s^{-1}.
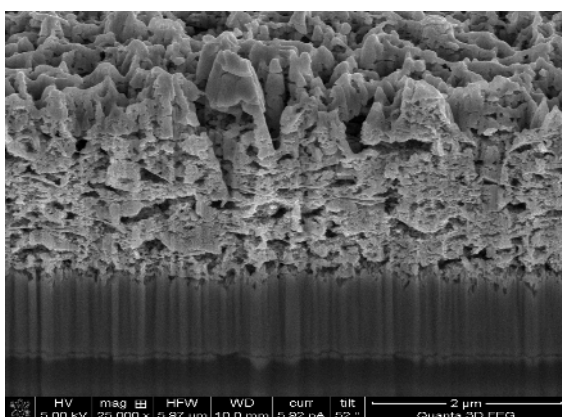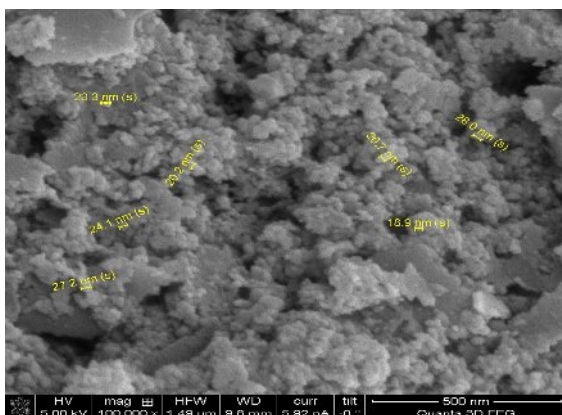

Fig. 6: SEM images of RDS sintered NiO coating with thickness 2-3 mm: (top) surface and (bottom) cross-sectional view obtained using a FEG-SEM.
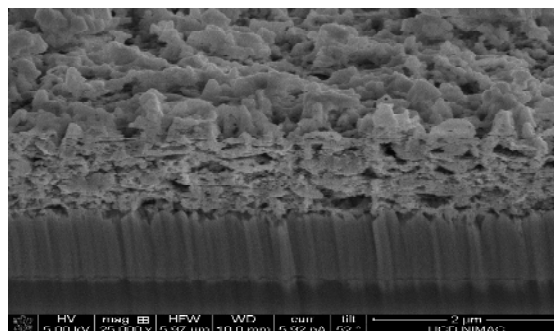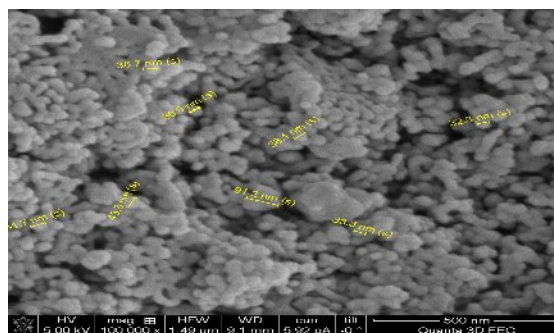

Fig. 7: SEM images of CS sintered NiO coating with thickness 2-3 mm: (top) surface and (bottom) cross-sectional view obtained using a FEG-SEM.

The electrochemical oxidation processes of ERY-sensitized NiO coatings are presented in Fig. 5. The integration of the current observed from anodic process related to the oxidation of dye-sensitized NiO coatings treated using RDS technique gave a charge of 2.53 mC cm^{-2} [42]. Whereas, ERY-sensitized NiO coatings sintered using the furnace gave a 0.58 mC cm^{-2} anodic charge. The resulting ratio of the charge exchanged by ERY-sensitized RDS treated NiO to that of furnace sintered NiO was approximately 4:1. However, the anodic charges exchanged by the sensitized coating were normally lesser than bare NiO coatings. This reduction of the exchanged charge could be due to a passivation effect of the ERY film towards the process of NiO oxidation. No change is evidenced in the voltage value for NiO oxidization in its transition from the uncovered (Fig. 4) to the sensitized state (Fig. 5). Therefore, it is concluded that sensitization of NiO coatings with ERY does not modify the state of the redox processes of bare NiO coatings. Moreover, the existence of the ERY dye results in a general decrease of the amount of charge associated with the redox process(es) of NiO. No additional redox peaks derived from the eventual electroactivity of the chemisorbed dye were detected within the examined range of potential applied [12, 45-47]. It defines that ERY performs a shielding effect on the oxidation of the supporting

NiO under dark conditions. In analogy with the trend observed for the bare oxide, the ERY-sensitized version of the RDS sample affords the largest current density (Fig. 5) and indicates that the sensitization of NiO with ERY has no effect on the extent of mesoporous structure of the as prepared samples.

Table-1: List of the parameters derived from the *J-V* characteristic curves of the *p*-DSCs with NiO photocathodes (RDS) **1** and (CS) **2** at different thickness values. Whereas ERY-1 stands for 5 min RDS treated NiO coatings used in *p*-DSCs; ERY-1*: 30 min RDS treated NiO coatings used in *p*-DSCs; ERY-2: Furnace Sintered (CS-treated) NiO coatings used in *p*-DSCs; electrolyte composition: 0.1M I_2, 1.0M LiI in acetonitrile; *l*: thickness; η: overall efficiency; V_{oc}: open circuit voltage; J_{sc}: short circuit current density and FF for fill factor.

Sample	l / μm	η / %	V_{oc} / V	$-J_{sc}$ / mA cm^{-2}	FF
ERY-1	0.6	0.008	0.102	0.169	0.464
ERY-1 (test 2)	0.6	0.014	0.130	0.290	0.370
ERY-1 (test 3)	0.6	0.015	0.130	0.330	0.360
ERY-1	2-3	0.045	0.120	1.050	0.360
ERY-1*	2-3	0.011	0.126	0.260	0.290
ERY-2	0.6	0.008	0.083	0.200	0.270
ERY-2	2-3	0.005	0.084	0.220	0.250

Characterization of p-DSCs

RDS and CS samples have been utilized as photocathodes in *p*-DSC solar cell employing ERY [12] as dye. The information of the corresponding *p*-DSCs is shown in Table-1. The *p*-DSCs produced using RDS treated NiO coatings show increased photovoltaic performance through the increase of both short-circuit current density (J_{sc}), and overall efficiency (η) with increasing thickness of the NiO layer up to an optimum value of l = 2-3 μm (Table 1). The *JV* characteristic curve of the *p*-DSC resulting from RDS treated NiO coating sensitized with ERY dye with 30 min sintering time has also been included for comparison purposes (Table 1) [43]. It is evident that for longer sintering times the RDS technique caused a vivid reduction in cathodic photocurrent, however does not affect considerably the photopotential (Table 1). The 5 min RDS-treated coatings clearly show a much better performance and indicate that the optimized RDS procedure here reported offers significant advantages in terms of saving energy for the fabrication of efficient *p*-DSCs. It should be noticed that the photovoltaic performance of the cell derived from the samples sintered for 30 min (2-3 μm thick) is rather alike with the cell constructed after 5 min sintering having a thickness of 0.6 μm. It advocates that for the case of sintered samples the real operative region showing photo-activity is opposite to the sintering time and that extended sintering diminishes mesoporosity with a resulting decrease of the electrode area accessible

for sensitization. The CS samples sensitized with ERY generate *p*-DSCs with performances that are weakly dependent on NiO electrode thickness as shown by V_{oc}, J_{sc} and η values that are practically unchanged when *l* passes from 0.6 to 2-3 μm (Table 1). Such a behavior shows the lack of direct proportionality between electrode thickness and the area of the electroactive surface. In fact, in passing from RDS to CS oxide we observe a general decrease of the open circuit voltage, V_{oc}, in the corresponding *p*-DSC (Table 1). Moreover, the value of V_{oc} is insensitive to the change of thickness for CS type samples. The combination of these features indicates that CS samples have a surface area which is not strongly dependent on film thickness. This could be a consequence of the minor porosity of CS NiO with respect to RDS NiO as partly confirmed by the comparison of the SEM pictures of NiO cross-sections (Fig.s 6 and 7) and BET analyses. In this context we should also analyze the mechanism of sintering for the two different modalities of heating of the NiO nanparticles in the deposited slurry. The mechanism of sintering differs for the two different modalities CS and RDS of sample heating. In the CS procedure the heat wave produced by the furnace proceeds from the surface of the sprayed deposit to the bulk of the NiO film. In the RDS procedure the heat wave has a verse of propagation that goes from inside the bulk to the external surface of NiO slurry due to the fine focalization of the microwave radiation inside the bulk of the deposit when this is immersed in a plasma atmosphere. Such a difference warrants the nanoporosity of the RDS sample throughout the whole film of NiO whereas the CS procedure is effective in imparting the feature of mesoporosity mostly in the external part of the film. Thicker films of CS NiO might suffer of the lack of mesoporosity and become too compact in their bulk for being very effective for the application of *p*-DSC. It is therefore concluded that the CS samples do not possess mesoporous features throughout the whole layer when *l* exceeds 1 μm. When the performances of the *p*-DSCs assembled with both sintered samples of equal thickness is compared the higher values of J_{sc} and η of the devices based on RDS treatment reflect the larger surface area of RDS samples with respect to CS samples. Although the best performing cell in this study is similar to what has already been reported previously [43], however in this work this trend is consistent with the results presented in Fig.s 4 and 5, which refer directly to the redox activity of the NiO film itself, and are explainable in terms of larger electroactive area of the RDS samples in comparison to CS samples (*vide supra*).

Conclusions

This work continues to explain the application of microwave plasma sintering (or rapid

discharge sintering, RDS) on the processing of NiO cotings to be used as photocathodes in *p*-type dye-sensitized solar cells having erythrosine B as dye-sensitizer. The photoelectrochemical and photovoltaic performances of the coatings obtained via RDS treatments were compared with that of the NiO coatings obtained through the sintering with a conventional furnace (CS treatment). A twofold increase in the electroactivity of bare NiO coatings was observed for RDS treated coatings to that of furnace sintered coatings. In addition the RDS treated ERY sensitized NiO coatings have shown four times more electroactivity in comparison with furnace sintered NiO coatings. By comparing photovoltaic performance of different *p*-DSCs that using NiO coatings with diverse thicknesses and sintering conditions, it was observed that RDS samples give a considerably better photovoltaic performance than CS samples of equal thickness. A possible explanation is the smaller grain size and more open mesoporous structure (giving larger surface area) of the RDS NiO with respect to CS NiO with beneficial effects on the overall efficiency, short-circuit current density and fill factor.

Acknowledgments

References

1. A. Cho, Energy's Tricky Tradeoffs, *Science*, **329**, 786 (2010).
2. http://science.nasa.gov/science-news/science-at-nasa/2002/solarcells/, (accessed Apr 2015).
3. A. G. Aberle, Thin-Film Solar Cells, *Thin Solid Films*, **517**, 4706 (2009).
4. B. O'Regan and M. Grätzel, A Low-Cost, High-Efficiency Solar Cell Based on Dye-Sensitized Colloidal TiO$_2$ films, *Nature*, **353**, 737 (1991).
5. A. Yella, *et al.*, Porphyrin-Sensitized Solar Cells with Cobalt (II/III)–Based Redox Electrolyte Exceed 12 Percent Efficiency, *Science*, **334**, 629 (2011).
6. J. Burschka, N. Pellet, S. J. Moon, R. Humphry-Baker, P. Gao, M. K. Nazeeruddin and M. Gratzel, Sequential Deposition as a Route to High-Performance Perovskite-Sensitized Solar Cells, *Nature*, **499**, 316 (2013).
7. J. H. Heo, *et al.*, Efficient Inorganic-Organic Hybrid Heterojunction Solar Cells Containing Perovskite Compound and Polymeric Hole Conductors, *Nat. Photonics*, **7**, 486 (2013).
8. G. E. Eperon, V. M. Burlakov, P. Docampo, A. Goriely and H. J. Snaith, Morphological Control for High Performance, Solution-Processed Planar Heterojunction Perovskite Solar Cells, *Adv. Funct. Mater.*, **24**, 151 (2014).
9. M. A. Green, A. Ho-Baillie, and H. J. Snaith, The Emergence of Perovskite Solar Cells, *Nat. Photonics*, **8**, 506 (2014).
10. F. Hao, C. C. Stoumpos, D. H. Cao, R. P. Chang, and M. G. Kanatzidis, Lead-Free Solid-State Organic-Inorganic Halide Perovskite Solar Cells, *Nat. Photonics*, **8**, 489 (2014).
11. M. A. Green, K. Emery, Y. Hishikawa, W. Warta, and E. D. Dunlop, Solar Cell Efficiency Tables (Version 45), *Prog. Photovoltaics Res. Appl.*, **23**, 1 (2015).
12. J. He, H. Lindström, A. Hagfeldt, and S. E. Lindquist, Dye-Sensitized Nanostructured Tandem Cell-First Demonstrated Cell with a Dye-Sensitized Photocathode, *Sol. Energy Mat. Sol. C.*, **62**, 265 (2000).
13. T. N. Murakami and M. Grätzel, Counter Electrodes for DSC: Application of Functional Materials as Catalysts, *Inorg. Chim. Acta*, **361**, 572 (2008).
14. J. He, H. Lindstrom, A. Hagfeldt and S. E. Lindquist, Dye-Sensitized Nanostructured *p*-Type Nickel Oxide Film as a Photocathode for a Solar Cell, *J. Phys. Chem. B*, **103**, 8940 (1999).
15. L. Li, E. A. Gibson, P. Qin, G. Boschloo, M. Gorlov, A. Hagfeldt, and L. Sun, Double-Layered NiO Photocathodes for *p*-Type DSSCs with Record IPCE, *Adv. Mater.*, **22**, 1759 (2010).
16. J. M. Ball, M. M. Lee, A. Hey, and H. J. Snaith, Low-Temperature Processed Meso-Superstructured to Thin-Film Perovskite Solar Cells, *Energy Environ. Sci.*, **6**, 1739 (2013).
17. H. Sato, T. Minami, S. Takata, and T. Yamada, Transparent Conducting *p*-type NiO thin Films Prepared by Magnetron Sputtering, *Thin Solid Films*, **236**, 27 (1993).
18. Y. M. Lu, W. S. Hwang, J. S. Yang, and H. C. Chuang, Properties of Nickel Oxide Thin Films Deposited by RF Reactive Magnetron Sputtering, *Thin Solid Films*, **420**, 54 (2002).
19. E. Fujii, A. Tomozawa, H. Torii and R. Takayama, Preferred Orientations of NiO Films Prepared by Plasma-Enhanced Metalorganic Chemical Vapor Deposition, *Jpn. J. Apl. Phys. 2*, **35** (1996).
20. W. C. Yeh and M. Matsumura, Chemical Vapor Deposition of Nickel Oxide Films from bis-n-Cyclopentadienyl-Nickel, *Jpn. J. Apl. Phys. 1*, **36**, 6884 (1997).
21. L. Berkat, L. Cattin, A. Reguig, M. Regragui, and J. C. Bernède, Comparison of the Physico-Chemical Properties of NiO Thin Films Deposited by Chemical Bath Deposition and by Spray Pyrolysis, *Mater. Chem. Phys.*, **89**, 11 (2005).
22. B. A. Reguig, A. Khelil, L. Cattin, M. Morsli and J. C. Bernède, Properties of NiO Thin Films Deposited by Intermittent Spray Pyrolysis Process, *Appl. Surf. Sci.*, **253**, 4330 (2007).

23. J. Moscovici, I. Bouessay, A. Rougier, and A. Michalowicz, Characterization by XAS of NiO Thin Films Prepared by Pulsed LASER Deposition, *Phys. Scripta*, 326 (2005).

24. B. Sasi and K. G. Gopchandran, Preparation and Characterization of Nanostructured NiO Thin Films by Reactive-Pulsed Laser Ablation Technique, *Sol. Energy Mat. Sol. C.*, **91**, 1505 (2007).

25. Y. Y. Xi, D. Li, A. B. Djurisic, M. H. Xie, K. Y. K. Man, and W. K. Chan, Hydrothermal Synthesis vs Electrodeposition for High Specific Capacitance Nanostructured NiO films, *Electrochem. Solid St.*, **11**, D56 (2008).

26. X. H. Xia, J. P. Tu, J. Zhang, X. L. Wang, W. K. Zhang, and H. Huang, Morphology Effect on the Electrochromic and Electrochemical Performances of NiO Thin Films, *Electrochim. Acta*, **53**, 5721 (2008).

27. A. Nakasa, H. Usami, S. Sumikura, S. Hasegawa, T. Koyama, and E. Suzuki, A High Voltage Dye-Sensitized Solar Cell using a Nanoporous NiO Photocathode, *Chem. Lett.*, **34**, 500 (2005).

28. E. A. Gibson, A. L. Smeigh, L. Le Pleux, J. Fortage, G. Boschloo, E. Blart, Y. Pellegrin, F. Odobel, A. Hagfeldt, L. Hammarström, A *p*-Type NiO-Based Dye-Sensitized Solar Cell with an Open-Circuit Voltage of 0.35 V, *Angew. Chem. Int. Edit.*, **48**, 4402 (2009).

29. P. Qin, J. Wiberg, E. A. Gibson, M. Linder, L. Li, T. Brinck, A. Hagfeldt, B. Albinsson, and L. Sun, Synthesis and Mechanistic Studies of Organic Chromophores with Different Energy Levels for *p*-Type Dye-Sensitized Solar Cells, *J. Phys. Chem. C*, **114**, 4738 (2010).

30. S. Passerini, B. Scrosati, and A. Gorenstein, The Intercalation of Lithium in Nickel Oxide and its Electrochromic Properties, *J. Electrochem. Soc.*, **137**, 3297 (1990).

31. M. Awais, M. Rahman, J. M. Don MacElroy, N. Coburn, D. Dini, J. G. Vos, and D. P. Dowling, Deposition and Characterization of NiOx Coatings by Magnetron Sputtering for Application in Dye-Sensitized Solar Cells, *Surf. Coat. Tech.*, **204**, 2729 (2010).

32. L. Le pleux, B. Chavillon, Y. Pellegrin, E. Blart, L. Cario, S. Jobic, and F. Odobel, Simple and Reproducible Procedure to Prepare Self-Nanostructured NiO Films for the Fabrication of *p*-type dye-Sensitized Solar Cells, *Inorg. Chem.*, **48**, 8245 (2009).

33. A. Nattestad, M. Ferguson, R. Kerr, Y. B. Cheng, and U. Bach, Dye-Sensitized Nickel (II) Oxide Photocathodes for Tandem Solar Cell Applications, *Nanotechnology*, **19** (2008).

34. K. W. Tan, M. Eng. Thesis, *Commercialization potential of dye-sensitized mesoscopic solar cells*, Massachusetts Institute of Technology, (2008).

35. M. Grätzel, Conversion of Sunlight to Electric Power by Nanocrystalline Dye-Sensitized Solar Cells* 1, *J. Photoch. Photobio.* A, **164**, 3 (2004).

36. R. McConnell, Assessment of the Dye-Sensitized Solar Cell, *Renew. Sust. Energ. Rev.*, **6**, 271 (2002).

37. A. P. Breen, B. Twomey, G. Byrne, and D. P. Dowling, Comparison Between Microwave and Microwave Plasma Sintering of Nickel Powders, *Mater. Sci. Forum*, **672**, 289 (2011).

38. B. Twomey, A. Breen, G. Byrne, A. Hynes, and D. P. Dowling, Rapid Discharge Sintering of Nickel-Diamond Metal Matrix Composites, *J. Mater. Process. Tech.*, **211**, 1210 (2011).

39. E. A. Gibson, M. Awais, D. Dini, D. P. Dowling, M. T. Pryce, J. G. Vos, G. Boschloo and A. Hagfeldt, Dye Sensitised Solar Cells with Nickel Oxide Photocathodes Prepared via Scalable Microwave Sintering, *Phys. Chem. Chem. Phys.*, **15**, 2411 (2013).

40. M. Awais, Ph.D. Thesis, *Deposition and Evaluation of Nickel Oxide Coatings for Dye-sensitized Solar Cell Application*, University College Dublin, (2011).

41. M. L. McConnell, D. P. Dowling, C. Pope, K. Donnelly, A. G. Ryder, and G. M. O'Connor, High Pressure Diamond and Diamond-Like Carbon Deposition using a Microwave CAP Reactor, *Diam. Relat. Mater.*, **11**, 1036 (2002).

42. M. Awais, E. Gibson, J. G. Vos, D. P. Dowling, A. Hagfeldt and D. Dini, Fabrication of Efficient NiO Photocathodes Prepared via RDS with Novel Routes of Substrate Processing for *p*-Type Dye-Sensitized Solar Cells, *ChemElectroChem*, **1**, 384 (2014).

43. M. Awais, M. Rahman, J. M. Don MacElroy, D. Dini, J. G. Vos, and D. P. Dowling, Application of a Novel Microwave Plasma Treatment for the Sintering of Nickel Oxide Coatings for Use in Dye-Sensitized Solar Cells, *Surf. Coat. Tech.*, **205,** Supplement **2**, S245 (2011).

44. G. Boschloo and A. Hagfeldt, Spectroelectrochemistry of Nanostructured NiO, *J. Phys. Chem. B*, **105**, 3039 (2001).

45. M. Awais, D. Dini, J. M. Don MacElroy, Y. Halpin, J. G. Vos, and D. P. Dowling, Electrochemical Characterization of NiO Electrodes Deposited via a Scalable Powder Microblasting Technique, *J. Electroanal. Chem.*, **689**, 185 (2013).

46. M. Awais, D. Dowling, M. Rahman, J. Vos, F. Decker and D. Dini, Spray-Deposited NiO x Films on ITO Substrates as Photoactive Electrodes for *p*-Type Dye-Sensitized Solar Cells, *J. Appl. Electrochem.*, **43**, 191 (2013).

47. V. Novelli, M. Awais, D. P. Dowling, and D. Dini, Electrochemical Characterization of Rapid Discharge Sintering (RDS) NiO Cathodes for Dye-Sensitized Solar Cells of *p*-Type, *Am. J. Anal. Chem.*, **6**, 176 (2015).